Journal of Materials Chemistry C

Accepted Manuscript

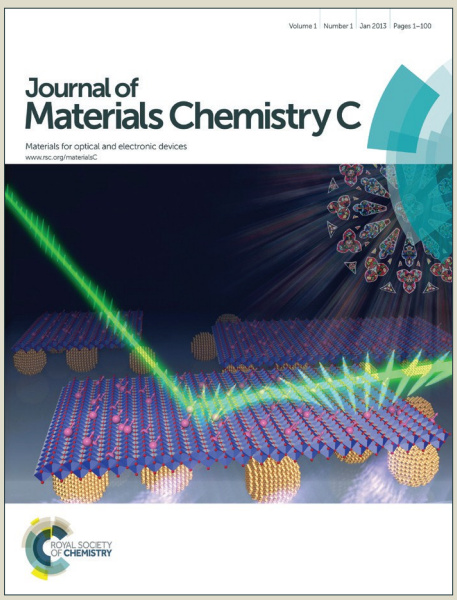

ROYAL SOCIETY OF CHEMISTRY

www.rsc.org/materialsC

Journal of Materials Chemistry C

ARTICLE

New Highly efficient electrochemical synthesis of dispersed Ag_2O particles in the vicinity of the cathode with controllable size and shape

Received 00th January 20xx,
Accepted 00th January 20xx

DOI: 10.1039/x0xx00000x

www.rsc.org/

Quoc-Thai Pham,[a,b] Bui The Huy,[a] Yong Ill Lee [*,a]

ABSTRACT: Silver (I) oxide (Ag_2O) hexapod particles were electrochemically synthesized with high efficiency in an aqueous solution of silver nitrate and sodium sulfate. The generation of dispersed Ag_2O particles in the vicinity of the cathode was explained by a two-step reaction mechanism involving the reduction of water, $2H_2O + 2e^- \rightarrow H_2 + 2OH^-$, followed by the precipitation of Ag_2O particles, $2Ag^+ + 2OH^- \rightarrow Ag_2O + H_2O$. The applied potential played an important role in controlling the size and yield of the Ag_2O hexapods. The average size of the hexapod particles was adjusted from 1.84 down to 0.60 μm by increasing the applied potential from 4 to 10 V. Furthermore, the ratio of the Ag_2O/Ag that was produced was determined to be ca. 23 when the applied potential was increased up to 10 V. On the other hand, the morphological change exhibited by the Ag_2O particles was determined to be a function of the silver ion concentration, which is proportional to the growth rate. The Ag_2O hexapods formed as a consequence of fast growth along the equivalent <100> directions.

Introduction

Silver oxide occurs in several forms and the following compounds have been defined: Ag_2O, AgO, Ag_2O_3, and Ag_3O_4. Among these, Ag_2O is the most stable[1] and is a known p-type semi-conductor with band gap energy of *ca.* 1.4 eV. The different crystal structures of Ag_2O offer a variety of interesting physicochemical properties, such as catalytic, electrochemical, electronic, and optical properties. As a result, these products have been widely used in many applications, such as in the catalytic oxidation of both hydroquinone[2] and carbon monoxide,[3] the water splitting reaction,[4] as a sensor for the detection of ammonia,[5,6] in photovoltaic cells,[7] in fuel cells,[8] and as a cathode in zinc—silver oxide batteries.[9-12]. As it is possible to adjust the optical properties of Ag_2O nanostructures by controlling their morphology, Ag_2O nanostructures with different morphologies, namely, cubes, rhombicuboctahedra, and hexapods have been synthesized.[13,14] Among them, the hexapods have received particular interest due to their unique morphology and optical properties.

The chemical preparation of silver oxide hexapods has been achieved by reacting silver ions (Ag^+) with hydroxide ions (OH^-) in the presence of ammonia, pyridine, or *bis*-(p-sulfonatophenyl)phenylphosphine dihydrate dipotassium to control the morphological shapes.[13-16] Silver oxides (*e.g.,* Ag_2O and AgO) can also be prepared by depositing thin films of these compounds using direct-current reactive magnetron sputtering techniques.[1,17-21] Nevertheless, the gas-phase synthesis requires high growth temperatures leading to limit the choice of substrate materials on which the silver oxide can be deposited. More importantly, it is difficult to obtain the silver oxide as either pure Ag_2O or AgO.

Electrochemical synthesis offers the most attractive approach for preparing micro- and nanostructured silver oxide at lower temperatures (*e.g.,* room temperature). Previous literature has reported the electrochemical synthesis of silver oxides as thin films[7] or micro- and naostructures[22, 23] deposited on the anode. Anodic oxidation has been found to result in the production of the mixture of silver oxide compounds (i.e., Ag_2O, AgO, Ag_2O_3) when overpotential is applied,[22, 24, 25] thus, the Ag_2O produced in this way is impure. It should be noted that dispersed Ag_2O micro- and nanoparticles have been electrochemically synthesized in the vicinity of the anode involving the anodic dissolution of silver electrode to produce Ag^+, followed by the precipitation of Ag_2O in a basic aqueous solution.[26] However, the dispersed Ag_2O particles were generated in the potential range from 0.25 to 0.85 V vs. Ag_2O/OH^-. To the best of our knowledge, the electrochemical synthesis of dispersed Ag_2O particles in the vicinity of the cathode has not yet been described in the literature. In this work, we present a new electrochemical strategy for the preparation

[a] *Department of Chemistry, Changwon National University, Changwon 641-773, Korea. E-mail: yilee@changwon.ac.kr*
[b] *Faculty of Chemical Engineering, Industrial University of HochiminhCity, Viet Nam.*
†Electronic Supplementary Information (ESI) available: Figures S1-3; Video 1. See DOI: 10.1039/x0xx00000x

of dispersed Ag_2O particles of specified sizes and shapes in the vicinity of the cathode. The Ag_2O particles were generated using the reduction of water molecules to provide OH^-. It was followed by immediate precipitation of Ag_2O near the cathode via reaction of OH^- and Ag^+ in the aqueous solution. The different applied potentials and concentrations of Ag^+ were carried out to control the size, shape, and yield of the Ag_2O particles.

Results and discussion

Once the potential (4, 5, 6, 8, or 10 V) is applied across the two electrodes, brown-colored dispersed Ag_2O particles can be observed to appear immediately in the vicinity of the cathode and precipitate from the solution, while a light gray-colored silver deposit is seen to accumulate on the cathode. By contrast, at an applied potential of 2 V, the only visible change at or near the cathode was the deposition of silver on the electrode itself. The key aspect of the generation of dispersed Ag_2O particles is a two-step mechanism involving the reduction of water molecules on the cathode to generate hydroxide anions. This is followed by the precipitation of Ag_2O in the vicinity of the cathode via the reaction of OH^- and Ag^+ in the solution. The reaction scheme is as follows:

$$2H_2O + 2e^- \rightarrow H_2 + 2OH^- \quad (1)$$

$$2Ag^+ + 2OH^- \rightarrow Ag_2O + H_2O \quad (2)$$

The calculated threshold potential for the water electrolysis cell is 1.48V. Therefore, the precipitation of Ag_2O, as shown in reaction 2, would be possible at applied potentials higher than 1.48 V. Thus, in this work an applied DC potential range from 2 to 10 V was adopted for the electrochemical process. The possible reason for generations of both deposited Ag and dispersed Ag_2O in the applied potential range from 4 to 10 V is that competition occurs between the formation of Ag_2O (reactions 1 and 2) in the vicinity of the cathode and the deposition of metallic silver on the cathode ($Ag^+ + e^- = Ag$, with a standard reduction potential E_0 = 0.799 V/NHE).

The weight ratios of Ag_2O/Ag obtained from the electrochemical processes in the applied potential range of 2 to 10 V at a silver ion concentration of 20 mM and 0.4 M Na_2SO_4 over a period of 10 min are shown in Fig. 1a. It can be seen that the ratio of Ag_2O/Ag (wt/wt) first increases significantly up to the point ($Ag_2O/Ag \approx 23$) at which the applied potential reached 8 V, beyond which the ratio is seen to stabilize irrespective of a further increase in the potential. This is most likely due to the extension of a zone that favors Ag_2O precipitation as a result of an increased presence of OH^- anions, which are generated by the reduction of water during the electrolysis. As illustrated schematically in Fig. 1b, the existence of the expected OH^- concentration gradient in

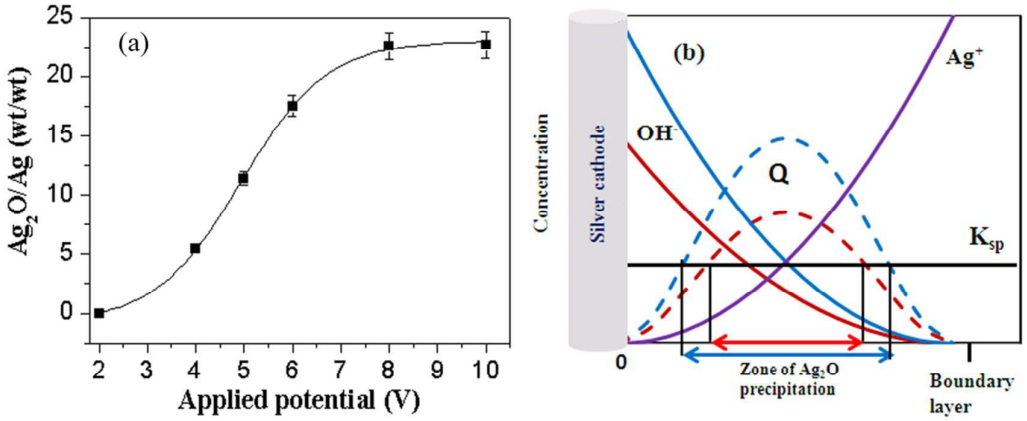

Fig. 1 (a) Plot of Ag_2O/Ag versus the applied potential for the electrochemical synthesis of Ag_2O in the vicinity of the cathode at the concentration of silver ion of 20 mM over a period of 10 min, (b) Schematic plot of concentration versus distance from silver cathode within boundary layer. Blue and red curves are the expected concentration gradients for OH^- at relatively high and low potentials, respectively, and purple curve concentration gradient for Ag^+. Also plotted is Q (dashed red or dashed blue curve at relatively low or high potential) the reaction quotient for reaction: $Ag_2O + H_2O \rightarrow 2Ag^+ + 2OH^-$ ($Q = [Ag^+]^2[OH^-]^2$). Ag_2O will precipitate within a zone in which the solubility product for Ag_2O, K_{sp}, exceeds Q, as indicated.

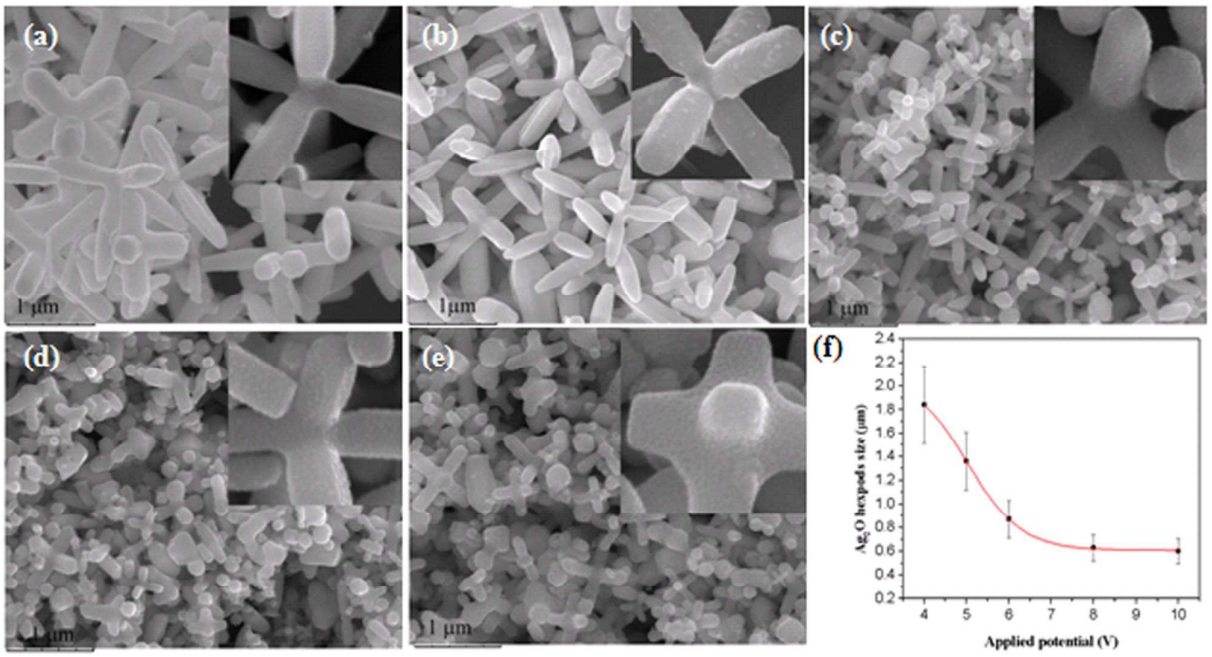

Fig. 2 FE-SEM images for the Ag_2O hexapods synthesized at the silver ion concentration of 20 mM for 10 min, and different potentials (a) 4 V, (b) 5 (V), (c) 6 V, (d) 8 V and (e) 10 V; (f) the average particle size versus the applied potential. The inset is higher magnification, showing the rough surface of hexapods particles.

the proximity of the surface of the cathode as a result of the reduction of water at relatively low (red curve) or high (blue) potential and the concentration gradient of Ag^+ (purple) can qualitatively explain the homogeneous precipitation of Ag_2O particles. At the same time, the deposition of dark-gray silver oxide(s) (Ag_xO) on the anode via an anodic oxidation process[7, 22-25] is also observed. However, the yield of silver oxides
generated anodically is very low compared to that of the dispersed Ag_2O obtained in the vicinity of the cathode, as confirmed by the following example. For the electrochemical process consisting of an aqueous solution of 0.4 M Na_2SO_4 containing 20 mM $AgNO_3$ conducted at an applied potential of 5 V for 10 min, the corresponding weight of dispersed Ag_2O generated in the vicinity of the cathode and the weight of Ag_xO deposited on the anode are 16 mg and 0.6 mg, respectively. This result demonstrates that the electrochemical synthesis of Ag_2O in the vicinity of the cathode is more efficient than the process leading to the deposition of Ag_xO on the anode under similar experimental conditions. The current experimental strategy is also highly scalable, because of the highly efficient process in which Ag_2O is generated, which makes it suitable for actual application. It is very interesting to note that the current method was successfully applied to the electrochemical synthesis of other metallic oxides (*e.g.,* zinc oxide nanosheet and nanorod).

The surface morphologies of dispersed Ag_2O particles obtained from the electrochemical process associated with the applied potential range of 4 to 10 V were characterized by using the field emission scanning electron microscopy (FE-SEM) images, and the results are shown in Fig. 2a-e. Geometrically, the Ag_2O particles consist almost entirely of hexapods (Fig 2a-c) at an applied potential of 4, 5, or 6 V. At higher potential of 8 or 10 V, the Ag_2O consists of hexapods and their fragments (see Fig. 2d, e). The average size of the Ag_2O hexapods plotted versus the applied potential is shown in Fig. 2f. Selected general features of these SEM images are briefly described here. The average sizes of the Ag_2O hexapods are 1.84, 1.36, 0.87, 0.63, and 0.6 μm at applied potentials of 4, 5, 6, 8, and 10 V, respectively. As shown in Fig. 2f, initially, the size of the Ag_2O hexapods decreases significantly down to a point at which the applied potential reaches 8 V, before leveling off despite a further increase in the potential. It is postulated that the decrease in the average size of the Ag_2O hexapods caused by the increase in the potential is essentially due to the greatly increased concentration of hydrogen molecules resulting from the electrolysis of water (reaction 1). Under the experimental circumstances, the hydrogen gas dispels the dispersed Ag_2O particles from within the zone of Ag_2O precipitation, in which the reactive Ag_2O particles are continuously able to grow, to the adjacent zone, which does not favor further growth (see ESI Video 1† for supporting information, the observation of hydrogen bubbles that immediately dispel the brown-colored Ag_2O particles from the cathode region to the adjacent zone when the potential applied).

A powder sample of Ag_2O hexapods obtained by electrochemical synthesis with a silver ion concentration of 20 mM and different applied potentials (4 or 10 V) characterized by using the X-ray diffraction (XRD) pattern measurement. Figure 3 shows the XRD patterns for samples of Ag_2O hexapods. All the diffraction peaks for both of the samples of Ag_2O hexapods (Fig. 3a and b), are quite similar; hence, they were assigned to a cubic Ag_2O lattice (JCPDS 41-1104). The corresponding lattice constant is

4.716 Å based on the XRD pattern, which is comparable with that of the JCPDS data (4.726 Å). It shows that the intensity of the (111) peak predominates within the XRD pattern for Ag_2O hexapods. By

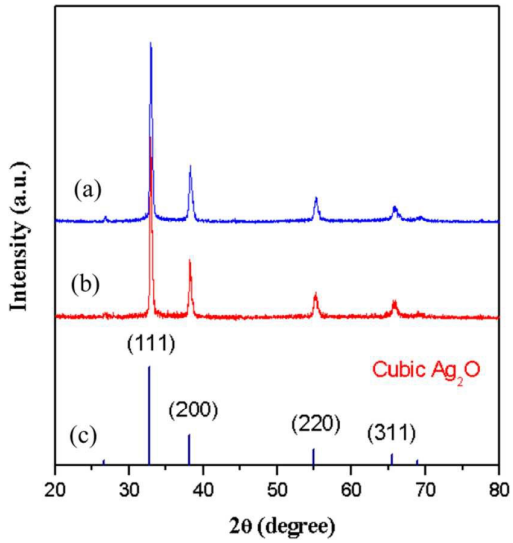

Fig. 3 XRD patterns for Ag_2O hexapod samples obtained at silver ion concentration of 20 mM, applied potentials of (a) 4 V and (b) 10 V; (c) JCPDS data (41-1104) for a cubic-Ag_2O.

Table 1. Binding energy of Ag (3d) and O (1s) photoelectrons for Ag_2O hexapods obtained from electrochemical synthesis.

Sample	Binding energy (eV)	
	Ag ($3d_{5/2}$)	O (1s)
Ag_2O hexapods	367.9	529.5
Ag[25]	368.3	
Ag_2O[7,25]	367.9	529.4
AgO[7, 25]	367.5	528.7, 531.6

contrast, the XRD pattern data for the Ag_2O synthesized by way of anodic oxidation[7, 23] showed the (200) peak to be more intense than the (111) peak. It is also very interesting to note that Ag_2O (or Cu_2O) crystals with exposed {111} faces contain positively charged silver (or copper) atoms at the surface, whereas the {100} faces are electrically neutral. In this regard, Ag_2O (or Cu_2O) hexapod particles with essentially revealed {111} faces were demonstrated to be more effective at photocatalytic reactions than the particles containing {100} faces.[13, 27, 28] The deposited silver is also confirmed by XRD pattern (see ESI Fig. S1†)

The electronic states and the band gap energies of samples of Ag_2O hexapods were evaluated by using the X-ray photoelectron spectroscopy (XPS) and UV-Vis measurements, respectively. First, the electronic states of the Ag_2O hexapods were examined on Ag (3d) and O (1s) (see Table 1 and ESI Fig. S2†). The Ag ($3d_{5/2}$) and O (1s) peaks were observed at binding energies of 367.9 and 529.5 eV, respectively. These values are consistent with those for Ag_2O in the literature (the binding energies of Ag ($3d_{5/2}$) = 367.9 eV and O (1s) = 529.4 eV).[7, 26] Figure 4 shows the UV-Vis-NIR spectrum of the Ag_2O hexapod particles, which, after some mathematical manipulation of both the absorbance and wavelength data, could be transformed into a plot of $(\alpha E)^2$ versus E (see inset within Fig. 4), where, α and E are the optical absorption coefficient and photon energy, respectively. The band gap (Eg) was estimated to be 1.42 eV by extrapolating a linear part of the plots to $(\alpha E)^2 = 0$. This value corresponds to that published in previous reports (Eg = 1.46 eV).[7, 13]

In order to gain a better understanding of the growth mechanism of an Ag_2O hexapod, we conducted a study using field emission transmission electron microscopy (TEM) and high-resolution TEM (HR-TEM) images of Ag_2O hexapods. Figure 5a shows that the Ag_2O hexapods can be aggregated from a large quantity of small particles serving as the building blocks. Figure 5b shows the magnification of an individual tip of a typical hexapod shown in Fig. 5a, showing the fine building block with a size of ca. 10 nm. The rough surfaces of the Ag_2O hexapods strongly suggest that there is a change of crystallization mechanism from classical ion-by-ion to the non-classical meso-scale assembly.[23, 29, 30] The selected-area electron diffraction (SAED) pattern measured on an individual tip (Fig. 5c), shows the characteristic polycrystalline rings consisting of a number of diffraction spots, each arising from the Bragg reflection of an individual crystallite. These results indicate that the Ag_2O hexapods are polycrystalline in nature and composed of a large quantity of building units with a size of ca. 10 nm, with each building unit most likely being a nanocrystal. The HR-TEM image (Fig. 5d) taken at the edge of a tip reveals the crystallographic orientation in the building block. The interplanar distances were measured to be 0.271 nm and 0.235 nm, which could be indexed to the {111} and {200} planes for a cubic Ag_2O lattice, respectively. The HR-TEM image exposed the existence of a {111} twin plane (marked by a dashed line) in the structure. We also observed the {-111} and {200} planes parallel to the two {-111} and {200} side faces of building unit, respectively. This result implies that the reactive building unit is a polyhedron, which exposes the equivalent {111} and {200} faces. Based on the HR-TEM study, it shows that the resulting hexapod could primarily be grown

Fig. 4 UV-Vis-NIR spectrum of the Ag_2O hexapod particles. The inset is the plot of $(\alpha E)^2$ versus photon energy (E).

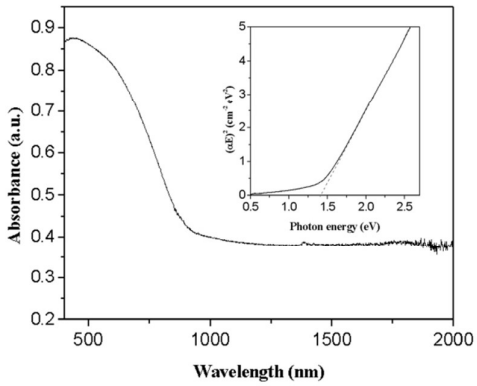

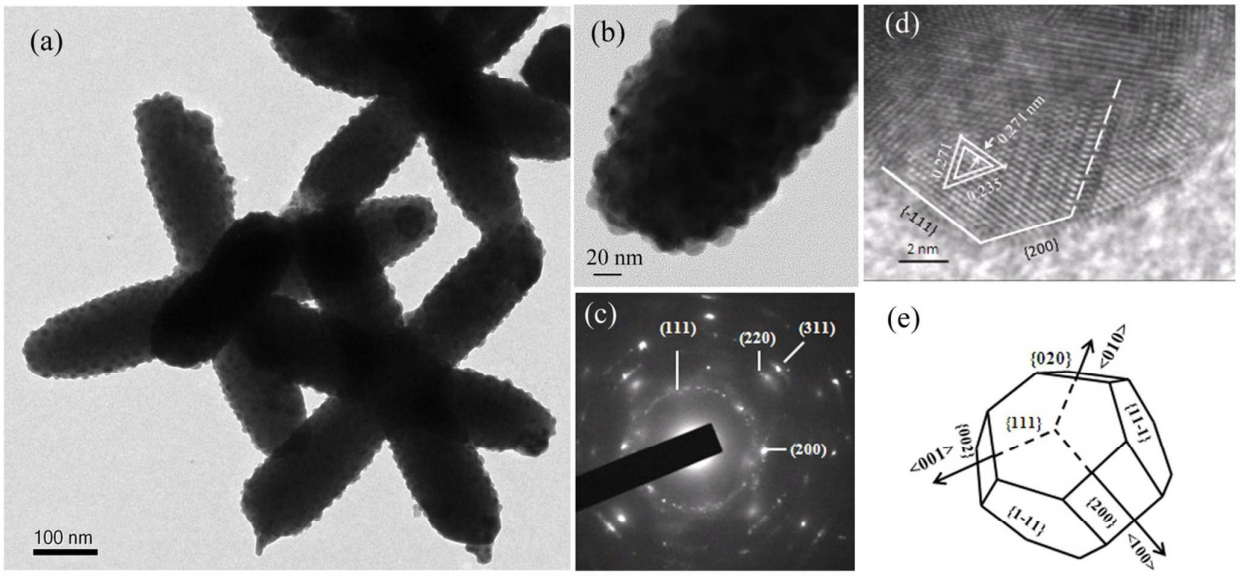

Fig. 5 (a) TEM image of Ag_2O hexapods synthesized at the silver ion concentration of 20 mM and the applied potential of 5 V, (b) at higher magnification showing rough surfaces, (c) SAED pattern obtained from one tip of a typical hexapod, (d) HR-TEM image taken at the edge of one tip in (b) and (e) illustration for a primary building block and growth directions along equivalent <100> directions.

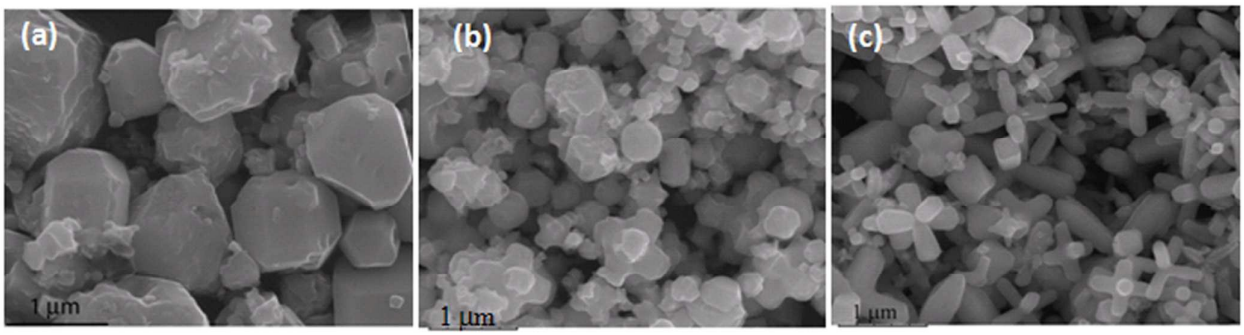

Fig. 6 FE-SEM images for Ag_2O particles obtained from electrochemical synthesis at constant potential of 5 V for 10 min with

from the equivalent {111} and {200} planes of the reactive building units, which form growth directions along the equivalent <100> directions, as illustrated in Fig. 5e.

the various silver ion concentrations (a) 1mM, (b) 5 mM and (c) 10 mM.

The change in the shape of the Ag_2O particles was also studied by using other silver ion concentrations (1, 5, and 10 mM). The SEM images for the Ag_2O particles obtained from the electrochemical synthesis at the same applied potential of 5 V associated with the various Ag^+ concentrations are shown in Fig. 6. At the lowest Ag^+ concentration (1 mM), the Ag_2O particles attained the shape of polyhedrons. Further, as the Ag^+ concentration was increased to 20 mM, the geometrical shape of the Ag_2O particles gradually changed from polyhedrons to shapes consisting entirely of hexapods (see Figs. 6a-c and 2b). In addition, the size of the Ag_2O hexapods were also observed to increase with an increasing silver ion concentration; for example, the size of the Ag_2O hexapods increased from less than 1 μm to *ca.* 1.36 μm when the Ag^+ concentration was increased from 10 to 20 mM (see Figs. 2b and 6c). This result indicates that the morphological change from a polyhedron to an Ag_2O hexapod is a function of the concentration of silver ions, which is proportional to the precipitation (growth) rate of the Ag_2O particles. In isotropic crystallization, the shape of a crystal grown in solution is thermodynamically defined by minimizing the interface energy and the surface energies of all the exposed faces (Wulff construction).[31, 32] The evolution of the shape from cubic to octahedral is a function of the ratio (R) of the growth rate along the <100> direction versus that along the <111> direction. The highest value of R = 1.73 results in an octahedron, whereas, the lowest value of R (0.58) produces a cube. A particle with a value between these two extremes, *i.e.,* 0.58 < R < 1.73, has exposed {111} and {100} faces, and is referred to as a polyhedron.[33] In particular, for isotropic face-centered cubic (FCC) Ag crystals, the thermodynamic equilibrium shape should be a convex polyhedron bounded by {111} and {100} planes.[34] By contrast, when a change occurs in the gradient of concentration, the interface morphology loses its stability and the branch will be raised.[35] Liu et al.[36] pointed out that the concave Ag hexapod shape is not the equilibrium one, and it formed in the fast growth synthesis. This is consistent with the fast growth rate observed for the Ag_2O hexapods during the electrochemical synthesis.

Conclusions

We have explored an unusual electrochemical methodology for synthesizing dispersed Ag_2O particles in the vicinity of the cathode. It was shown that the size, shape, and yield of Ag_2O particles can be controlled by manipulating both the applied potential and the silver ion concentration. The Ag_2O particles were generated in close proximity to, but in contact with, the cathode, provided the applied potential exceeded the threshold potential for the electrolysis of water. The higher the applied potential, the higher the yield and the smaller the particle size of the Ag_2O attained. That is, the size of the dispersed Ag_2O hexapods can be adjusted from 1.84 down to 0.60 μm by increasing the applied potential from 4 to 10 V at a constant silver ion concentration (20 mM). The current strategy is highly scalable due to the high efficiency and high yield of the process by which the micro-scale Ag_2O particles are generated, which means it is suitable for the actual application. Furthermore, the current method could be extended to the electrochemical synthesis of other metallic oxides (*e.g.,*ZnOnanosheet or nanorod).

Experimental

Silver (I) oxide particles were electrochemically synthesized in aqueous, 1-20 mM silver nitrate ($AgNO_3$, 99,9%, Kojima chemicals) in combination with 0.4 M sodium sulfate (Na_2SO_4, +99%, Junsei) at room temperature (ca. 25 ^oC). The synthesis was carried out using a two-electrode system comprising two silver rods (3.175 mm diameter, 99.9%, Alfa), separated by a distance of 3 cm, that served as anode and cathode, respectively. When the potential (4, 5, 6, 8 or 10 V) was applied across the two electrodes, brown-colored dispersed Ag_2O particles were observed to appear immediately in the vicinity of the cathode and precipitate from the solution, while a light gray-colored silver deposit was seen to adhere on the cathode. By contrast, at an applied potential of 2 V, the only deposition of silver was seen on the electrode. The Ag particles attached on the cathode and the dispersed Ag_2O particles were easily separated by lifting the cathode from the solution.

The final products were collected by centrifugation, followed by washing with ultrapure water for further investigation.

The morphological features of Ag_2O particles were characterized by using field emission scanning electron microscopy (FE-SEM, MIRA II LMH, Tescan) and field emission transmission electron microscopy (TEM, JEM2100F model, JEOL, operating at 200 kV). The Ag_2O powder samples were confirmed by using X-ray diffraction (XRD, X'PERT, PANalytical, Cu Kαradiation) pattern measurement. Electronic states of Ag_2O powder were evaluated by using X-ray photoelectron spectroscopy (XPS, Multilab 2000, Thermo Scientific, Al Kα radiation). Binding energies were corrected using the C (1s) line at 284.5 eV. XPS analysis was performed with monochromated Al Kα radiation at pressure ca. 1.5×10^{-8} Pa. The band gap energy of Ag_2O particles was determined via UV-Vis-NIR (V-670 JASCO) measurement.

Acknowledgements

This work was supported by the Region University Research Program (NRF 2014-008793) and the Priority Centers Program (NRF 2010-0029634) through the National Research Foundation of Korea (NRF) funded by the Ministry of Education, Science and Technology.

References

1 J. F. Pierson and C. Rousselot, *Surf. Coat. Technol.* 2005, **200**, 276–279.
2 F. Derikvand, F. Bigi, R. Maggi, C. G. Piscopo and G. Sartori, *J. Catal.,* 2010, **271**, 99–103.
3 G. A. El-Shobaky, M. A. Shouman and S. M. El-Khouly, *Mater. Lett.,* 2003, **58**, 184–190.
4 W. Wang, Q. Zhao, J. Dong and J. Li, *Int. J. Hydrogen. Energ.,* 2011, **36**, 7374–7380.
5 B. J. Murray, Q. Li, J. T. Newberg, J. C. Hemminger and R. M. Penner, *Chem. Mater.* 2005, **17**, 6611–6618.
6 V. V. Petrov, T. N. Nazarova, A. N. Korolev and N. F. Kopilova, *Sensor. Actuator.* B 2008, **133**, 291–295.
7 Y. Ida, S. Watase, T. Shinagawa, M. Watanabe, C. Chigane, M. Inaba, A. Tasaka and M. Izaki, *Chem. Mater.,* 2008, **20**, 1254–1256.
8 E. Sanli, B. Z. Uysal and M. L. Aksu, *Int. J. Hydrogen. Energ*., 2008, **33**, 2097–2104.
9 K. T. Braan, S. K. Volkman andV. Subramanian, *J. Power Sources*, 2012, **199**, 367–372.
10 M. Mojtahedi, M. Goodarzi, B. Sharifi and J. V. Khaki, *Energ. Convers. Manage*., 2011, **52**, 1876–1880.
11 M. Venkatraman and J. W. V. Zee, *J. Power Sources*, 2007, **166**, 537–548.
12 X. Jin, and J. Lu, *J. Power Sources*, 2002, **104**, 253–259.
13 L. M. Lyu, W. C. Wang and M. H. Huang, *Chem. Eur. J*, 2010, **16**, 14167–14174.
14 L. M. Lyu and M. H. Huang, *Chem. Asian J.*, 2013, **8**, 1847-1853.
15 M. J. Kim, Y. S. Cho, S. H. Park and Y. D. Huh, *Cryst. Growth Des*., 2012, **12**, 4180−4185.
16 J. Jo, S. P. Cho and J. K. Lim, *J. Colloid. Interf. Sci.*, 2015, **448**, 208–214.
17 Y. C. Her, Y. C. Lan, W. C. Hsu andS. Y. Tsai, *J. Appl. Phys.* 2004, **96**, 1283–1288.
18 Y. Chiu, U. Rambabu, M. H. Hsu, H. P. D. Shieh, C. Y. Chen and H. H. Lin, *J. Appl. Phys.,* 2003, **94**, 1996–2001.
19 Y. Abe, T. Hasegawa, M. Kawamura and K. Sasaki, *Vacuum*, 2004, **76**, 1–6.
20 J. F. Pierson, D. Wiederkehr and A. Billard, *Thin Solid Films*, 2005, **478**, 196–205.
21 T. Arai, C. Rockstuhl, P. Fons, K. Kurihara, T. Nakano, K. Awazu and J. Tominaga, *Nanotechnology*, 2006, **17**, 79–82.
22 W. Wei, X. Mao, L. A. Ortiz and D. R. Sadoway, *J. Mater. Chem.*, 2011, **21**, 432-438.
23 J. Fang, P. M. Leufke, R. Kruk, D. Wang, T. Scherer and H. Hahn, *Nano Today*, 2010, **5**, 175–182.
24 T. P. Dirkse, Electrochim. Acta, 1990, **35**, 1445–1449.
25 T. P. Dirkse, Electrochim. Acta, 1989, **34**, 647–650.
26 B. J. Murray, Q. Li and J. T. Newberg,, E. J. Menke, J. C. Hemminger and R. M. Penner, Nano Lett., 2005, **5**, 2319–2324.
27 J. Y. Ho, and M. H. Huang, *J. Phys. Chem. C*, 2009, **113**, 14159–14164.
28 C. H. Kou and M. H. Huang, *J. Phys. Chem. C* 2008, **112**, 18355–18360.
29 H. Colfen and S. Mann, *Angew. Chem. Int. Ed.*, 2003, **42**, 2350 – 2365.
30 H. Colfen and M. Antonietti, *Angew. Chem. Int. Ed.*, 2005, **44**, 5576 – 5591.
31 G. Wulff, *Z. Kristallogr*., 1901, **34**, 449–530.
32 E. Ringe, R. P. V. Duyne and L. D. Marks, *Nano Lett.*, 2011, **11**, 3399–3403.
33 Z. L. Wang, *J. Phys. Chem. B,* 2000, **104**, 1153–1175.
34 J. W. M. Frenken and P. Stoltze, *Phys. Rev. Lett*., 1999, **82**, 3500–3503.
35 I. Sunaga, in *Crystals-Growth, Morphology and Perfection*; Cambridge University Press: Cambridge, 2005, ch. 3, pp. 20-59.
36 X. Liu, R. Huang and J. Zhu, *Chem. Mater.*, 2008, **20**, 192–197.

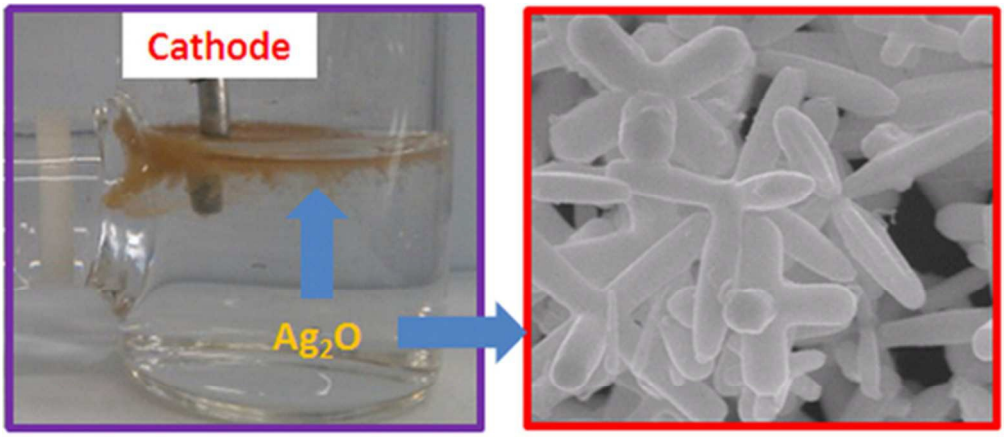

$$2H_2O + 2e \rightarrow H_2 + 2OH^-$$

$$2Ag^+ + 2OH^- \rightarrow Ag_2O + H_2O$$

45x26mm (300 x 300 DPI)